



HAL
open science

Corrosion of T91 and pure iron in flowing and static Pb-Bi alloy between 450 °C and 540 °C: experiments, modelling and mechanism

L. Martinelli, K. Ginestar, Valéry Botton, C. Delisle, F. Balbaud-Célérier

► To cite this version:

L. Martinelli, K. Ginestar, Valéry Botton, C. Delisle, F. Balbaud-Célérier. Corrosion of T91 and pure iron in flowing and static Pb-Bi alloy between 450 °C and 540 °C: experiments, modelling and mechanism. *Corrosion Science*, 2020, 176, pp.108897. 10.1016/j.corsci.2020.108897 . hal-03234703

HAL Id: hal-03234703

<https://hal.science/hal-03234703>

Submitted on 22 Aug 2022

HAL is a multi-disciplinary open access archive for the deposit and dissemination of scientific research documents, whether they are published or not. The documents may come from teaching and research institutions in France or abroad, or from public or private research centers.

L'archive ouverte pluridisciplinaire **HAL**, est destinée au dépôt et à la diffusion de documents scientifiques de niveau recherche, publiés ou non, émanant des établissements d'enseignement et de recherche français ou étrangers, des laboratoires publics ou privés.



Distributed under a Creative Commons Attribution - NonCommercial 4.0 International License

Corrosion of T91 and pure iron in flowing and static Pb-Bi alloy between 450°C and 540°C: experiments, modelling and mechanism

L. Martinelli^{a*}, K.Ginestar^a, V.Botton^b, C.Delisle^c, F.Balbaud-Célérier^a

^a *Université Paris-Saclay, CEA, Service de la Corrosion et du Comportement des Matériaux dans leur Environnement, 91191, Gif-sur-Yvette, France*

^b *CNRS UMR5509, LMFA, Université de Lyon, ECL, INSA Lyon, Université Lyon 1, 69134 Ecully, FRANCE.*

^c *Institut de recherche sur les lois fondamentales de l'univers (IRFU), CEA, Université Paris-Saclay, F-91191, Gif-sur-Yvette, France*

**: corresponding author
tel: +33 1 69 08 59 33
e-mail address: laure.martinelli@cea.fr*

Abstract:

T91 (Fe-9Cr steel) and pure iron were corroded in pure dissolution domain in liquid lead bismuth eutectic (LBE) from 450 to 540°C in static and in dynamic LBE flow. The modelling showed that corrosion rates were controlled: (i) for static condition (LBE natural convection), by the iron diffusion in the diffusion boundary layer; (ii) for flowing LBE, by a mixed process combining both the interfacial reaction rate of iron dissolution and the iron diffusion rate in the diffusion boundary layer. By fitting the modelling on the experimental points, the constant of interfacial reaction rate was determined.

Key words: corrosion mechanism (C), dissolution (C), diffusion (C), reaction rate (C), Pb-Bi (A), Fe-9Cr (A)

1 Introduction

Lead alloys, and particularly lead-bismuth eutectic (LBE), are considered as primary coolant in Pb-Bi cooled fast reactors and in Accelerator Driven Systems. However, lead alloys can be corrosive toward materials and particularly toward one of the ADS candidate structural material: the ferritic-martensitic Fe-9Cr steel, T91 [1]- [39]. T91 corrosion process depends on the concentration of oxygen dissolved in Pb-Bi. Indeed, for oxygen concentration lower than the one necessary for magnetite formation (approximately lower than 10^{-8} wt % at temperature around 500°C for Fe-9Cr steels), corrosion proceeds by dissolution of T91 [3][4][5][9][10][15][17][20][22][23][24][29][36][39] [40][41].

In this case, corrosion kinetics is not identified: Short *et al* [29] consider parabolic kinetics for F91 at 615 and 715°C while Gorynin *et al* [10] present linear kinetics. Moreover, processes controlling steel dissolution are not clearly determined. For instance, assuming a linear corrosion kinetics, Balbaud *et al.* [40][41] show that in flowing Pb-Bi, T91 dissolution rate is controlled by iron diffusion in the diffusion boundary layer at steel/Pb-Bi interface [40] and, in a more recent paper [41], by a mixed control process combining both iron diffusion and interfacial reaction of iron dissolution. On the other hand, Yamaki *et al.* [43] show that in static Pb-Bi, dissolution of 316L austenitic steel follows a linear kinetics and its corrosion rate is controlled by the interfacial reaction rate. Some modelling of steels dissolution/oxidation have been done [38]-[56] but few modelling exist on pure dissolution of the Fe-Cr steels [40][41][49][52][53][55][56]. Some of these modelling are mass transfer modelling [49][52][55][56], the one of Maulana *et al* is atomistic modelling [53], and the ones of Balbaud *et al* [40][41] are mechanistic modelling. The goal of mechanistic modelling is to identify the various corrosion stages (chemical reaction, diffusion...), to model them and to determine which stage controls the corrosion rate.

The aim of this paper is firstly to obtain a corrosion kinetics in order to identify if the corrosion kinetics is parabolic or linear. This corrosion kinetics will be done in static Pb-Bi conditions. Secondly, it is to perform mechanistic modelling of the corrosion rate, in dynamic Pb-Bi conditions. This modelling has to forecast the corrosion rate of T91 or pure iron whatever the temperature (between 450 and 550°C), the Pb-Bi velocity (in a range corresponding to 0-2.5 m/s for a 1cm diameter pipe) and the dissolved iron concentration in Pb-Bi.

This paper is the following of previous work [41] which showed that corrosion rate is controlled by a mixed process both limited by interfacial reaction rate and diffusion rate in the concentration boundary layer which thickness is fixed by the mass transfer coefficient (see part 5.). Then modelling the corrosion rate involves determining the interfacial reaction rate constant and the mass transfer coefficient in the geometry of the corrosion test. To conclude, the objective of this paper is:

- (i) first to present experimental corrosion kinetics in static Pb-Bi in order to determine if the kinetics is linear or parabolic;
- (ii) secondly, to present corrosion tests in flowing Pb-Bi in CICLAD facility [40][41];
- (iii) finally, to model the corrosion rate in case of static Pb-Bi and then of flowing Pb-Bi using the mass transfer coefficient determined by previous simulations with the Computational Fluid Dynamics (CFD) software Fluent™ [42]. This modelling will permit to assess the corrosion rate of pure Fe and T91 as a function of temperature and LBE flow velocity.

2 Symbols used in the paper

A : sample surface area (m^2)

a : constant

b : constant

$C_X^{LBE} (b)$: concentration of dissolved X in the LBE bulk ($mol\ cm^{-3}$)

$C_{X,eq}^{LBE}$: concentration of dissolved element X at thermodynamic equilibrium with X in the steel ($mol\ m^{-3}$)

³⁾

C_{ref}^{LBE} : reference concentration of dissolved element X in LBE ($mol\ m^{-3}$)

C_{ref}^S : reference concentration of element X in steel ($mol\ m^{-3}$)

$C_X^S(w)$: concentration of element X in steel at the solid/liquid interface ($mol\ m^{-3}$)

$C_X^S(bulk)$: concentration of element X in steel bulk ($mol\ m^{-3}$)

d : sample diameter in CICLAD facility (cm)

d_{pipe} : pipe diameter (cm)

D : diffusion coefficient of dissolved specie in liquid Pb-Bi ($cm^2\ s^{-1}$)

D_{Fe} : iron diffusion coefficient in Pb-Bi ($cm^2\ s^{-1}$)

D_X : diffusion coefficient of X in LBE

E : activation energy of dissolution rate constant (J mol^{-1})

g : gravitational acceleration (m s^{-2})

h : dissolved steel thickness (mm)

J : corrosion rate ($\text{mol cm}^{-2} \text{s}^{-1}$)

\vec{J}_{Conv} : convection flux ($\text{mol cm}^{-2} \text{s}^{-1}$)

\vec{J}_{Dif} : diffusion flux of the dissolved element X in the LBE diffusion boundary layer ($\text{mol cm}^{-2} \text{s}^{-1}$)

\vec{J}_{diss} : dissolution flux ($\text{mol cm}^{-2} \text{s}^{-1}$)

\vec{J}_T : transfer flux ($\text{mol cm}^{-2} \text{s}^{-1}$)

J_{Ty} : ordinate y of the transfer flux ($\text{mol cm}^{-2} \text{s}^{-1}$)

K : mass transfer coefficient (cm s^{-1})

k_d : dissolution rate constant ($\text{mol cm}^{-2} \text{s}^{-1}$)

k_d^0 : pre-exponential factor of the dissolution rate constant ($\text{mol cm}^{-2} \text{s}^{-1}$)

k_{pr} : precipitation rate constant ($\text{mol cm}^{-2} \text{s}^{-1}$)

M_X : molar mass of X element (g mol^{-1})

M_{T91} : T91 molar mass (g mol^{-1})

m_X^{LBE} : mass of dissolved X in LBE (g)

n_X^{LBE} : number of mole of dissolved X in LBE (mol)

Nu : Nusselt number,

R : gas constant ($\text{J mol}^{-1} \text{K}^{-1}$)

Re : Reynolds number

S_X : solubility limit of X in LBE (mol cm^{-3})

Sc : Schmidt number

Sh : Sherwood number

t : time (s)

T : temperature ($^{\circ}\text{C}$ or K)

\vec{V} : LBE flow rate (cm s^{-1})

X_{LBE} : dissolved steel element X in Pb-Bi

X_S : element X in the solid steel

β : LBE thermal dilation coefficient (K^{-1})

δ : diffusion boundary layer thickness (cm)

Δm_{T91}^{LBE} : T91 weight loss (g)

Δt : corrosion time (s)

η : dynamic viscosity (Pa s)

ν : kinematic viscosity ($cm^2 s^{-1}$)

ω angular velocity ($rad s^{-1}$)

ρ : density ($g cm^{-3}$)

3 Material and methods

3-1 Experimental procedures in CICLAD and COLIMESTA facilities

Dissolution experiments are performed in liquid lead-bismuth eutectic (LBE), from METALEUROP supplier, containing in wt%: 44.8% lead, 55.2% bismuth and in weight ppm: [Ag] = 5, [Fe] < 0.2, [Cu] < 0.7. Tests are carried out between 450 and 553°C using T91 martensitic steel from Industeel supplier and pure iron ARMCO® from Weber supplier. Compositions of T91 and Fe are given in Table 1. Before experiments T91 was subjected to a two steps heat treatment: (i) a normalisation step at 1050°C during 15 minutes followed by cooling in water; (ii) a tempering step at 770°C during 45 minutes followed by cooling in still air. T91 has been provided by the DEMETRA/EUROTRANS European Project.

Table 1: T91 and Fe compositions in weight percent (wt%). Iron is the balance.

Experiments are carried out in the CICLAD and the COLIMESTA devices [39]. These devices are designed to perform corrosion experiments, respectively in flowing and stagnant lead alloys. COLIMESTA consists of a tank containing 7L of LBE, in a glove box. CICLAD is a corrosion loop. Its test section consists also of a tank (containing 5L of LBE) in a glove box. Its loop is a circuit dedicated to the continuous purification of liquid alloy. Steel samples are rotating cylinders fixed to a rotating shaft as represented on Figure 1. The samples angular velocity can be adjusted between 35 and 450 $rad s^{-1}$.

Figure 1. CICLAD diagram.

Before being machined, T91 plate was annealed under vacuum at 1040 °C for 1 h, quenched and then tempered at 760 °C for 1 h to obtain the required ferritic–martensitic microstructure. COLIMESTA samples are small T91 rectangular sheets of approximate dimensions 30 mm x 10 mm x 1 mm. Specimens were ground to a 1200-grit surface finish and degreased ultrasonically in an acetone-ethanol mixture before use. Seven samples are immersed together in LBE at 552°C and removed at regular time interval.

CICLAD samples are T91 and pure iron small cylinders of approximate 8 mm diameter and approximate 20 mm length. Samples are mirror polished before corrosion tests. These tests are performed at 450, 470, 500, 540°C and 550°C (Table 2). Three samples can be held on the rotating shaft during experiments.

To keep constant the dissolved corrosion products concentrations in the LBE bulk, the CICLAD facility has a LBE purification loop, including a cold trap (Figure 1). The Fe concentration dissolved in the liquid alloy is measured before and after each experiment by sampling followed by ICP -AES (Perkin-Elmer Optima 2000 DV) analyses. In both experiments (COLIMESTA and CICLAD), Ar-4%vol H₂ gaseous mixture is continuously sweeping above liquid LBE in order to remove dissolved oxygen from liquid alloy. In both devices, an oxygen sensor, constituted by yttria doped zirconia (internal reference is Bi-Bi₂O₃ mixture) [39][64][65], is immersed in LBE. It allows a continuous measurement of dissolved oxygen (Table 2).

After experiments, solidified Pb-Bi is removed from the corroded samples by their immersion in a solution containing, in volume, 1/3 acetic acid, 1/3 hydrogen peroxide, 1/3 ethanol.

After solidified Pb-Bi removal, samples are weighed and some samples are coated by Ni (electrochemical method) to be protected from cutting and process preparation for Scanning Electron Microscopy (SEM) observations.

In the CICLAD device, to avoid destabilization of the liquid alloy flow by presence of obstacles, revolution symmetry is achieved by adding a hollow cylinder containing the rotating shaft: the oxygen sensor and the gas inlet tubes are not enclosed in the rotating LBE flow (Figure 1).

LBE flow is modelled by CFD software which permits calculation of mass transfer coefficient in CICLAD facility. This determination is detailed in [42].

Table 2: Experimental conditions and results.

4 Results

4-1 Corrosion experiments in COLIMESTA

Figure 2 is a SEM picture of a cross section of T91 corroded 400 h in COLIMESTA at 552°C. Two corrosion zones are observed: one corresponding to slight corrosion (Figure 2a) and the other corresponding to accelerated corrosion (Figure 2b).

Figure 2. SEM picture of cross section of T91 corroded 400 h in COLIMESTA device at 552°C. Two zones, (a) and (b) are noticeable: (a) slight corrosion zone; (b) accelerated corrosion zone.

Figure 3. EDX map of an accelerated corrosion zone (see Figure 2b) of T91 corroded 400 h in COLIMESTA device at 552°C. (a) SEM-QBSD picture. The profile line corresponds to the EDX profile of Figure 4; (b) Fe map; (c) Cr map.

Figure 3 and Figure 4 show that, at the steel/ Pb-Bi interface, the ratio of iron concentration over the chromium concentration seems constant and very close to the its value in the steel. Consequently, for T91 the dissolutions of Cr and Fe are congruent.

Figure 4. EDX profile of profile line presented on Figure 3a. Presence of Ni corresponds to Ni deposit performed after test.

Figure 5 represents the corrosion kinetics obtained at 552°C in Pb-Bi under natural convection (COLIMESTA). It shows that corrosion kinetics is linear. The corrosion rate is then constant and, considering the values presented on Figure 5, equal to $6 \times 10^{-5} \text{ g m}^{-2} \text{ s}^{-1}$, or equal to 245 $\mu\text{m/year}$ considering a T91 density equal to 7.8 g cm^{-3} .

Figure 5. T91 weight loss per surface area (mg cm^{-2}) towards time (h). Experiment performed in COLIMESTA at 552°C . Modelling is performed considering pure mass transfer control.

As observed in Figure 5, the corrosion kinetics intersects the t-axis at 175 h. This intersection coordinate is usually [43] considered as the duration needed to dissolve the original passive layer and to wet the sample. This duration is called wetting time or incubation time in some papers.

4-2 Corrosion experiments in CICALAD

As the corrosion kinetics is linear in “static” conditions (natural convection in fact) and thus the corrosion rate is constant, the corrosion rate in CICALAD (forced convection) is also considered as constant [41] for the two following reasons. First the dissolved iron and chromium concentrations are constant, due to the purification loop and to the great Pb-Bi volume. Secondly the Pb-Bi flow reaches a steady state according to CFD calculation [42], mass transfer coefficient is constant. The CICALAD facility has thus been used to study the evolution of the corrosion rate with temperature and flow velocity: three samples are corroded in the same time for one duration, one angular velocity and one temperature. The corrosion rate is calculated by the weight loss over the corrosion duration. To avoid impact of wetting time on corrosion rate, a wetting step of the samples was performed. During this wetting step, the three cylindrical samples are immersed (without any rotation) together with two sheets of the same material (T91 or pure Fe) in Pb-Bi during 48 h at 470°C . After these 48 hours, the two sheets are removed and weighed. If a weight loss is measured, dissolution of the original passive layer and sample wetting are assumed. The experiment can begin: temperature is fixed at the wanted value and when this temperature is reached, rotation of the samples begins. If the weight loss is zero, the sheets are again immersed, together with the cylindrical samples, 48h in Pb-Bi at 470°C .

At the end of the experiment, the samples’ weight losses are measured; the weight loss per surface area due to the wetting step is removed and the corrosion rate is determined from the beginning of the samples rotation. The corrosion rate is the evaluated weight loss per surface area divided by the corrosion time. The assumption, that cylindrical samples are totally wetted (and not only partially) at the experiment beginning, is one of the higher uncertainty in the corrosion rate measurement. Indeed, some parts of samples are not wetted after the test. This feature leads to a heterogeneity in the dissolution depth as observed in Figure 2. In this SEM image, some residual LBE is also observed. This LBE presence tends

to slightly under estimate the corrosion rate however its effect can be neglected in comparison to the heterogeneous dissolution. The two main uncertainties are thus: (i) the wetting time and (ii) the corroded surface area approximated to the sample surface area.

Figure 6 presents the results of the corrosion rate of samples corroded in the CICLAD facility as a function of the angular velocity of the rotating shaft. Samples used are usually pure iron but some experiments have also been made with T91 (for 56 and 107 rad s⁻¹ at 470°C, for 232 rad s⁻¹ at 540°C); these latter are plotted with empty symbols.

Figure 6. Corrosion rate (mg m⁻² s⁻¹) of T91 and pure iron at 450, 470, 500 and 540°C. Open symbols correspond to T91 samples, full symbols to pure Fe samples. Numbers 1, 2, 3 correspond respectively to the upper sample, the sample in the middle and the lower sample on the rotating shaft.

Figure 6 shows that the corrosion rate increases when angular velocity increases, excluding experiment at (540°C ; 440 rad s⁻¹) plotted here as round symbols and for which concentration of dissolved iron was higher than for the other experiments (Table 2). Corrosion rate also increases with temperature. An important dispersion in the results is observed. This difference is not due to the sample localization on the rotating shaft as observed on Figure 6. It could be partly explained by a difference of wetting which affects the corroded area used for calculation of corrosion rate. Summary of corrosion results are given in Table 2.

Table 2 shows that the corrosion rates of T91 seem similar to the corrosion rate of pure iron as previously shown by Balbaud [40].

5 Modelling of corrosion rate and discussion

5-1 Modelling of corrosion rate

Figure 7a from [68] represents the three fluxes involved in steel dissolution in Pb-Bi:

(i) the first flux, \vec{J}_{diss} , is the dissolution flux that is the dissolution rate of interfacial reaction:



with X_s , the solid steel element, X_{LBE} the dissolved steel element in the lead-bismuth eutectic (LBE), k_d the reaction rate constant for X_s dissolution and k_{pr} the reaction rate constant for X_{LBE} precipitation.

(ii) The second flux, \vec{J}_{Dif} , is the diffusion flux of the dissolved element X_{LBE} through the diffusion boundary layer of thickness δ (Figure 7b). This flux is perpendicular to steel surface.

(iii) The third flux, \vec{J}_{Conv} , is the convection flux which carries the dissolved element X_{LBE} across the liquid bulk if there is convection. This convection can be natural or forced. Dissolved species are thus transported (considering the transfer flux, \vec{J}_T (Figure 7a)) to the bulk of the fluid successively by diffusion through the boundary layer and by convection outside the boundary layer.

Figure 7. (a) diagram of the 3 fluxes involved in dissolution process (b) diagram representing iron concentration gradient in the diffusion boundary layer [68].

Considering these different fluxes, the corrosion mechanism is modelled.

The dissolution flux is written in one dimension, considering a homogeneous dissolution; it is collinear to the y-axis:

$$\vec{J}_{diss} = J_{diss} \vec{y} = J_{diss} \Rightarrow J_{diss} = k_d \frac{C_X^S(w)}{C_{ref}^S} - k_{pr} \frac{C_X^{LBE}(w)}{C_{ref}^{LBE}} \quad (15)$$

For sake of simplicity, values of C_{ref}^S and C_{ref}^{LBE} are chosen in order that $k_d = k_{pr}$.

At chemical equilibrium, $J_{diss} = 0$ and the concentration of X in LBE at the wall interface reaches its solubility limit: $C_X^{LBE}(w) = S_X$. By convenience we will take $C_{ref}^{LBE} = S_X$. The ratio $\frac{C_X^S(w)}{C_{ref}^S}$ has thus to be equal to 1 at chemical equilibrium. As the dissolution of Cr and Fe are congruent, the concentration of X in the solid at the wall interface, $C_X^S(w)$, is always equal to its content in the solid bulk, we will then take $C_{ref}^S = C_X^S(bulk)$ in order to have $\frac{C_X^S(w)}{C_{ref}^S}$ always equal to 1.

Then, according to (15), J_{diss} , is written:

$$J_{diss} = k_d \left(1 - \frac{C_X^{LBE}(w)}{S_X} \right) \quad (16)$$

The transfer flux, \vec{J}_T , is (Figure 7):

$$\bar{J}_T = -\frac{C_X^{LBE} D_X}{RT} \bar{\nabla} \mu_X + C_X^{LBE} \bar{V} \quad (17)$$

With D_X the diffusion coefficient of X in LBE, T the temperature in K, R the gas constant, μ_X the chemical potential of dissolved X in LBE and \bar{V} the LBE flow rate. This flux is represented on Figure 7a. The ordinate y of this flux is (Figure 7b):

$$J_{Ty} = -D_X \frac{\partial C_X^{LBE}}{\partial x} \quad (18)$$

Introducing the concentration boundary layer thickness δ and the mass transfer coefficient K , equation (18) becomes:

$$J_{Ty} = D_X \frac{C_X^{LBE}(w) - C_X^{LBE}(b)}{\delta} = K(C_X^{LBE}(w) - C_X^{LBE}(b)) \quad (19)$$

With $C_X^{LBE}(w)$ the concentration of dissolved X at the steel/LBE interface (wall interface) and $C_X^{LBE}(b)$ the concentration of dissolved X in the LBE bulk.

CICLAD purification loop is considered sufficiently efficient to neglect the increase of dissolved X concentration due to steel dissolution. Then at steady state, dissolved X concentration in LBE is constant as a function of time and the dissolution flux is equal to the ordinate y of the transfer flux, i.e the diffusion flux ($J_{Ty} = J_{diss} = J$). Then equality of equations (16) and (19) leads to the concentration, $C_X^{LBE}(w)$, of dissolved X at the steel/LBE interface:

$$C_X^{LBE}(w) = \frac{k_d + K C_X^{LBE}(b)}{k_d / S_X + K} \quad (20)$$

And combining (20) and (16) or (19), the flux, J ($J_{Ty} = J_{diss} = J$), becomes:

$$J = \frac{k_d K}{k_d + S_X K} (S_X - C_X^{LBE}(b)) \quad (21)$$

Then according to the second Fick's law, the molar dissolution rate, $\frac{1}{A} \frac{dn_X^{LBE}}{dt}$ (with A the steel sample surface area and n_X^{LBE} the molar quantity of dissolved X in LBE), is written:

$$J = \frac{1}{A} \frac{dn_X^{LBE}}{dt} = \frac{1}{AM_X} \frac{dm_X^{LBE}}{dt} = \frac{k_d K}{k_d + S_X K} (S_X - C_X^{LBE}(b)) \quad (22)$$

With m_X^{LBE} the mass of dissolved X in LBE and M_X the molar mass of X element.

Considering equation (22), if LBE flow velocity is sufficiently low that mass transfer coefficient is much lower than dissolution rate constant ($S_X K < k_d$), corrosion rate is controlled by diffusion of X in the diffusion boundary layer and equation (22) becomes:

$$\frac{1}{AM_X} \frac{dm_X^{LBE}}{dt} = K(S_X - C_X^{LBE}(b)) \quad (23)$$

According to equation (22), when LBE flow velocity increases, mass transfer coefficient increases and then the corrosion rate increases.

Otherwise, if the LBE flow velocity is sufficiently high that product of mass transfer coefficient and X solubility limit in LBE is much higher than the dissolution rate constant ($S_X K > k_d$), corrosion rate is controlled by the rate of interfacial dissolution reaction and equation (22) becomes:

$$\frac{1}{AM_X} \frac{dm_X^{LBE}}{dt} = \frac{k_d}{S_X} (S_X - C_X^{LBE}(b)) \quad (24)$$

According to equation (24), when LBE flow velocity increases, steel corrosion rate remains constant.

In the case of dissolution of pure iron and of T91, the involved diffusion coefficient and solubility limits are those of iron:

(i) the iron diffusion coefficient, D_{Fe} , in pure lead is assumed to be equal to that in LBE:

$$D(m^2 s^{-1}) = 4.9 \cdot 10^{-7} \exp\left(-\frac{43935}{RT}\right) \quad [66]$$

(ii) and the iron solubility limit in LBE, S_{Fe} , is:

$$S_{Fe} (mol / m^3) = 18.27 \exp\left(-\frac{10085.3}{T}\right) (11065 - 1.293T) \quad [69].$$

According to this study's results and to literature [40], the corrosion rates of T91 and pure iron are similar. The T91 corrosion kinetics is thus controlled by dissolution and diffusion of iron.

In order to model the corrosion rate, the rate of interfacial dissolution reaction, k_d and the mass transfer coefficient, K , have to be determined. The mass transfer coefficient has been determined by mass transfer simulation (see section 5-2) and the rate of interfacial dissolution reaction, k_d , will be fitted on experimental results.

5-2 Mass transfer coefficients in CICLAD and COLIMESTA

5-2-1 Mass transfer coefficient in CICLAD experiment

Mass transfer coefficient in CICLAD has been determined at 470°C by CFD modeling in previous study [42]. It will be considered, in the following that the mass transfer coefficients at temperatures from

450 to 540°C are similar to the one calculated at 470°C. Three trends are given as a function of the flow velocity (Re^2Sc ; with $Re = \frac{\omega d^2}{2\nu}$ and $\nu = \frac{\nu}{D}$):

$$K = 1.9 \times 10^{-1} \left(\frac{\omega^2 d^4}{4\nu D_{Fe}} \right)^{0.31} \frac{D_{Fe}}{d} \text{ for } 2 \times 10^9 < Re^2 Sc < 5.3 \times 10^{10}; \quad (25)$$

$$K = 1.4 \times 10^{-3} \left(\frac{\omega^2 d^4}{4\nu D_{Fe}} \right)^{0.51} \frac{D_{Fe}}{d} \text{ for } 5.3 \times 10^{10} < Re^2 Sc < 8.5 \times 10^{11}; \quad (26)$$

$$K = 1.1 \times 10^{-2} \left(\frac{\omega^2 d^4}{4\nu D_{Fe}} \right)^{0.43} \frac{D_{Fe}}{d} \text{ for } 8.5 \times 10^{11} < Re^2 Sc < 10^{13}. \quad (27)$$

with D_{Fe} : iron diffusion coefficient in LBE, ν : kinematic viscosity, d : diameter of cylindrical samples; ω : angular velocity.

5-2-2 Determination of mass transfer coefficient for COLIMESTA experiment

For COLIMESTA geometry, thermal analogy is also done to calculate the mass transfer coefficient. COLIMESTA is a cylindrical tank in which samples are immersed. The natural convection is calculated assuming two infinite horizontal planes in which a temperature gradient exists between the top (colder) and the bottom (hotter). Temperatures at the bottom and the top of the tank are respectively 553°C and 551°C, leading to a temperature difference $\Delta T = 2$ °C. Then the mass transfer coefficient is given by [62]:

$$K = 0.069 (g\beta\Delta T)^{1/3} \nu^{-0.259} D^{0.593} \frac{H}{d} \quad (28)$$

With ΔT , the temperature difference between the top and the bottom of the tank, g the gravitational acceleration, β the LBE thermal dilation coefficient ($1.25 \cdot 10^{-4} \text{K}^{-1}$ [39]).

According to (28) the mass transfer coefficient value in COLIMESTA is estimated to be: $K = 2.38 \cdot 10^{-6} \text{ m s}^{-1}$.

5-3 *Discussion: comparison experiments-modelling*

Taking into account equation (23) considering a pure mass transfer control and equation (28) for the determination of the mass transfer coefficient ($K = 2.38 \cdot 10^{-6} \text{ m s}^{-1}$) the weight loss is calculated as a

function of time for COLIMESTA experiments, assuming that the dissolved iron concentration, $C_{Fe}^{LBE}(b)$, is negligible toward S_{Fe} (see Table 3 for the numerical applications):

$$\frac{\Delta m_{T91}^{LBE}}{A} = KM_{T91}S_X t \quad (29)$$

Equation (29) is presented together with experimental kinetics performed in COLIMESTA device in Figure 5.

Table 3: Parameters needed for modelling the corrosion rate in COLIMESTA and CICLAD devices.

Figure 5 shows that modelling considering pure mass transfer control is twice as fast as the experimental results. Considering uncertainties in experimental results, it could be concluded that corrosion rate is purely mass transfer controlled. This means that iron diffusion in the concentration boundary layer due to natural convection controls the corrosion rate in COLIMESTA experiment.

For CICLAD experiments, the experimental corrosion rate divided by the difference between iron solubility limit and iron concentration in the LBE bulk $\left(\frac{1}{AM_{Fe/T91}} \frac{\Delta m_X^{LBE}}{\Delta t} \frac{1}{(S_{Fe} - C_{Fe}^{LBE}(b))}\right)$ is presented on Figure 8 (see also Table 2) as a function of the samples rotation speed. As the physical value plotted in y-axis is not the corrosion rate but the corrosion rate divided by iron solubility which increases with temperature, this value decreases when temperature increases.

The modelling corresponding to mixed process presented together with experimental points on Figure 8 is given by equations (22) and (25), (26) or (27) depending on the angular velocity ω

$$\frac{1}{AM_{Fe/T91}} \frac{\Delta m_X^{LBE}}{\Delta t} \frac{1}{(S_{Fe} - C_{Fe}^{LBE}(b))} = \frac{k_d K}{k_d + S_{Fe} K} \quad (30)$$

The only unknown data of equation (30) is the reaction rate constant k_d . It is determined by superimposition of equation (30) on experimental data considering that its dependence with temperature follows an Arrhenius law: $k_d = k_d^0 \exp\left(-\frac{E}{RT}\right)$, with k_d^0 the pre-exponential factor and E the activation energy.

Figure 8. Corrosion rate at various temperatures (from Figure 6) divided by the difference between iron solubility limit and iron concentration in the LBE bulk $\left(\frac{1}{AM_{Fe/T91}} \frac{\Delta m_X^{LBE}}{\Delta t} \frac{1}{(S_{Fe} - C_{Fe}^{LBE}(b))}\right)$ as a function of angular velocity. Modelling $\left(\frac{k_d K}{k_d + S_{Fe} K}\right)$ for the various temperatures (450, 470, 500, 540°C).

The best fit of modelling (equation (30)) on experimental results is given for:

$$k_d (\text{mol} \cdot \text{cm}^{-2} \cdot \text{s}^{-1}) = 1.22 \times 10^{-8} \text{Exp} \left(-\frac{9418}{RT} \right) \quad (31)$$

A simple sensitivity study shows that the modelling still fits on experimental results when the value of k_d is twice the one given by relation (31). This is due to the high dispersion of experimental results.

Modelling and experimental results are in good agreement for experiments at 540°C and 500°C but discrepancy between modelling and experiments increases when temperature decreases: for 470°C and then 450°C. For these two temperatures, experimental points have always lower corrosion rate than the calculated ones. This can be due to a partial dissolution of the passive layer at these lower temperatures. Indeed, the experimental corrosion rate is calculated (see section 4-2) considering a homogeneous dissolution. The corroded surface area is then over estimated leading to an underestimation of the experimental corrosion rate.

According to the CFD simulation the mass transfer coefficient is the same for the three samples (Figure 1). Then the discrepancy observed for the three samples in the same test is due to experimental dispersion, it means to the heterogeneity of the corrosion zones (Figure 2). Indeed, even after 400h of dissolution at 552°C, some parts of the specimen are scarcely corroded and some parts are clearly corroded. Moreover, as presented on Figure 2, some martensite laths are removed from the substrate because of a preferential dissolution on grain boundaries. This heterogeneous dissolution leads to distort the weight loss measurement and then the experimental corrosion rate.

The present calculations based on a homogeneous dissolution permitted to have a first estimation of the rate constant for reaction of dissolution. Sharper comprehension and modelling of the corrosion mechanism would permit to understand the heterogeneous corrosion pattern and then to have a better estimation of the local rate constant for dissolution reaction.

Moreover, looking at relation (22) the corrosion rate is proportional to $(S_x - C_x^{LBE}(b))$. Thus, the concentration of dissolved Fe in LBE is of first order on the corrosion rate variation. This concentration is determined by ICP-AES analyses on LBE samples before and after the test. This concentration value is questionable as: firstly the volume of LBE sample is about 1 cm³ and it can be not representative of the global volume of LBE that is 5 L in the CICLAD tank and 7 L in COLIMESTA. Secondly, sampling, for

ICP-AES analyses, are made after solidification (by quenching) of this volume. Consequently, even the sampling may not be totally representative of the 1 cm³ sample of LBE.

Consequently, a first estimation of the rate constant for reaction of dissolution, k_d , obtained by superimposition of modelling on experimental data, is given equation (31). This rate constant will permit to give estimation of the corrosion rate (in pure dissolution process, without oxidation) of T91 whatever the temperature and the angular velocity till 450 rad s⁻¹.

This reaction rate constant can be compared with the apparent dissolution rate of 316L obtained by Yamaki *et al* [43]:

$$k_d^{app316L} (mol\ cm^{-2}\ s^{-1}) = \frac{9.17 \times 10^{-6} M_{Ni}}{M_{316L} w_{Ni}} \text{Exp}\left(-\frac{7.83 \times 10^4}{RT}\right) = 9.17 \times 10^{-5} \text{Exp}\left(-\frac{7.83 \times 10^4}{RT}\right)$$

With w_{Ni} the weight fraction of Ni in 316L and $M_{316L/Ni}$ the molecular mass of 316L and Ni.

For instance at 500°C, $k_d^{app\ 316\ L}$ is equal to 4.7x10⁻¹⁰ mol cm⁻² s⁻¹ while the Fe dissolution rate constant, k_d , is equal to 5.3x10⁻⁸ mol cm⁻² s⁻¹. Considering corrosion controlled by the dissolution reaction rate, the maximum corrosion rate at 500°C (for $C_X^{LBE}(b)=0$) is equal to 0.1 mm/year for 316L and 6 mm/year for T91.

Then contrary to usual belief that nickel containing alloys have higher dissolution rate than Fe-Cr steels (as nickel solubility limit is much higher than iron and chromium solubility limits); it is shown by this study that the reaction rate of T91 is two orders of magnitude higher than the reaction rate of 316L. Thermodynamics cannot easily explain these differences in corrosion kinetics. It could be explained by the presence of addition elements in the 316L that decreases the dissolution reaction rate constant, k_d . Indeed, experiments of pure dissolution of austenitics show that their corrosion kinetics mainly depend on the element addition as they can impede dissolution of Ni [44]. More complex phenomena should thus be studied to understand this counter intuitive kinetics.

Regarding the mass transfer coefficient in CICALAD, it depends, according to CFD simulation, on the Re^2Sc range (see [42] and equations (25) to (27)). Considering that the mass transfer coefficient is constant and approximated to the one of equation (27) whatever the angular velocity, the modelling obtained is presented on Figure 9 together with the experimental results.

Figure 9. Corrosion rate at various temperatures (from Figure 6) divided by the difference between iron solubility limit and iron concentration in the LBE bulk $\left(\frac{1}{AM_{Fe/T91}} \frac{\Delta m_X^{LBE}}{\Delta t} \frac{1}{(S_{Fe} - C_{Fe}^{LBE}(b))}\right)$ as a function of angular velocity. Modelling $\left(\frac{k_d K}{k_d + S_{Fe} K}\right)$ for the various temperatures (450, 470, 500, 540°C). K is given only by equation (27) on the overall range of $Re^2 Sc$, i.e. of angular velocity ω k_d is given by the previous fit: $k_d (\text{mol cm}^{-2} \text{ s}^{-1}) = 1.22 \times 10^{-8} \text{Exp}\left(-\frac{9418}{RT}\right)$.

Figure 9 shows that this approximation is in good agreement with the experimental results.

Then relation (27) can then be used for all the angular velocities and relation (30) becomes, using equations (27) and (31):

$$\frac{1}{AM_X} \frac{dm_X^{LBE}}{dt} = \frac{1.342 \times 10^{-10} \text{Exp}\left(-\frac{9418}{RT}\right) \left(\frac{\omega^2 d^4}{4\nu D_{Fe}}\right)^{0.43} \frac{D_{Fe}}{d}}{1.22 \times 10^{-8} \text{Exp}\left(-\frac{9418}{RT}\right) + 1.1 \times 10^{-2} S_{Fe} \left(\frac{\omega^2 d^4}{4\nu D_{Fe}}\right)^{0.43} \frac{D_{Fe}}{d}} (S_{Fe} - C_{Fe}^{LBE}(b))$$

As in a real process, T91 is the structural material of pipe containing flowing LBE, the results obtained in this study must be adapted to pipe geometry.

5-4 Corrosion rate modelling for pipe geometry

Results and modelling in this study permitted to obtain the dissolution rate constant, k_d , that can now be injected in modelling adapted to a pipe geometry.

A critical review of the Sherwood numbers obtained for various geometries has been done by Silverman [70] who discussed the capability of making experiments with rotating cylinder electrodes to simulate corrosion in pipe. He underlined that such correlations can only be done if some assumptions are fulfilled: (i) the hydrodynamic and the concentration boundary layers are fully formed for the considered geometry; (ii) surfaces are smooth; (iii) interferences from end effects is absent; (iv) corrosion is homogeneous and does not depends on some particular shape and position.

In this study, the first assumption (the thickness of the concentration boundary layer is thinner than 300 μm and then fully formed), the third and the fourth assumptions are fulfilled for experiment and

modelling. For the experiments, the second assumption is not fulfilled as surfaces are not smooth (see Figure 2). However, for the CFD simulation surfaces are smooth. The equivalence between both smooth pipe and the smooth cylinder of CICLAD modelling by CFD will be done.

Several mass transfer coefficient are given by literature for pipe geometry [57][58][71][72]. The ones of Silverman [71][72] and Berger and Hau [57] lead to very similar results. According to Silverman they are based on the most reliable results [73]. As Silverman uses the Berger and Hau's [57] relation for its latest correlation [59], the mass transfer coefficient considered here for pipe geometry is the one of Berger and Hau [57]:

$$K_{B-H} = 0.0165V^{0.86}d_{pipe}^{-0.14}\nu^{-0.53}D_{Fe}^{0.67} \quad (32)$$

With V the Pb-Bi velocity, d_{pipe} the pipe diameter, ν the Pb-Bi kinematic viscosity and D_{Fe} the diffusion coefficient of Fe in liquid Pb-Bi.

According to relation (27) the mass transfer coefficient in CICLAD is:

$$K_{CICLAD} = 1.1 \times 10^{-2} \left(\frac{\omega^2 d^4}{4\nu D_{Fe}} \right)^{0.43} \frac{D_{Fe}}{d} \quad (33)$$

Equalizing (32) and (33), velocity in pipe can be expressed as a function of angular velocity:

$$V = 0.312 \omega d^{0.837} d_{pipe}^{0.163} \left(\frac{\nu}{D_{Fe}} \right)^{0.116} \quad (34)$$

Equation (34) shows that the link between pipe velocity and angular velocity depends on temperature. When temperature decreases, as Pb-Bi kinematic viscosity increases and iron diffusion coefficient in Pb-Bi decreases, pipe velocity increases for the same angular velocity.

Equations (30), (31) and (32) lead to the following corrosion rate:

$$\frac{1}{AM_X} \frac{\Delta m_X^{LBE}}{\Delta t} = \frac{2.013 \times 10^{-10} \text{Exp}\left(-\frac{9418}{RT}\right) V^{0.86} d_{pipe}^{-0.14} \nu^{-0.53} D_{Fe}^{0.67}}{1.22 \times 10^{-8} \text{Exp}\left(-\frac{9418}{RT}\right) + 0.0165 V^{0.86} d_{pipe}^{-0.14} \nu^{-0.53} D_{Fe}^{0.67} S_{Fe}} (S_{Fe} - C_{Fe}^{LBE}(b)) \quad (35)$$

Using values of Table 3, equation (35) leads, for T91, to:

$$\frac{dh}{dt} (m/s) = \frac{V^{0.86} \text{Exp}\left(-\frac{3540.57}{T}\right) \left(1.124 \times 10^{-12} T + 4.757 \times 10^{-14} C_{Fe}^{LBE}(b) \text{Exp}\left(-\frac{10085.3}{T}\right) - 9.618 \times 10^{-9}\right)}{-1.22 \times 10^{-4} d_{pipe}^{0.14} \frac{\text{Exp}\left(\frac{10484.97}{T}\right)}{(11065 - 1.293T)^{0.53}} + 1.01 \times 10^{-3} V^{0.86} (1.293T - 11065) \text{Exp}\left(-\frac{2407.78}{T}\right)} \quad (36)$$

With, V in (m/s), d_{pipe} in (m), T in (K), $C_{Fe}^{LBE}(b)$ the concentration of dissolved iron in (mol/m^3) in the liquid alloy. If this concentration, $C_{Fe}^{LBE}(b)$, is negligible towards the solubility limit S_{Fe} (mol/m^3), the corrosion rate is maximum and equal to:

$$\frac{dh}{dt}(\text{mm/year}) = \frac{V^{0.86} \text{Exp}\left(-\frac{3540.57}{T}\right) (3.544 \times 10^{-2} T - 303.3)}{-1.22 \times 10^{-4} d_{pipe}^{0.14} \frac{\text{Exp}\left(\frac{10484.97}{T}\right)}{(11065 - 1.293T)^{0.53}} + 1.01 \times 10^{-3} V^{0.86} (1.293T - 11065) \text{Exp}\left(-\frac{2407.78}{T}\right)}$$

(37)

With, V in (m/s), d_{pipe} in (m), T in (K).

Relation (37) is presented together with experimental results for which $C_{Fe}^{LBE}(b)$ is negligible (see Table 2) at 500°C and 540°C in Figure 10.

Figure 10. Corrosion rate at 500°C and 540°C (from Figure 9) as a function of pipe velocity.

Modelling, $\frac{dh}{dt}(\text{mm/year})$, considering relation (37).

Figure 10 shows that corrosion rate can be very high when dissolved iron concentration in Pb-Bi bulk is equal to zero even for low flow velocity. As iron solubility limit is very low ($7.5 \times 10^{-7} \text{ mol cm}^{-3}$ at 540°C), iron impurities dissolved in Pb-Bi can easily reach close concentrations and limit the corrosion kinetics as shown by experiments 9 and 12 in Table 2. Corrosion is then limited by the temperature difference between the coldest and the highest part of the circuit. The coldest part will fix the dissolved iron concentration.

CONCLUSION

This study shows pure Fe and T91 dissolution experiments in static and dynamic LBE conditions under very low dissolved oxygen concentration. Then models were made to forecast corrosion rate of T91 and pure iron, in pure dissolution domain, whatever the temperature and the LBE velocity.

In “static” condition, dissolution is linear as a function of time. Modelling shows that dissolution rate is controlled by natural convection.

In dynamic conditions:

(i) Experiments show that pure Fe and T91 corrosion rates, in pure dissolution domain, are the same (in agreement with [1]).

(ii) Simulations show that their corrosion rates are controlled by mixed phenomenon: that are both interfacial reaction and diffusion controls.

This model permitted to determine:

(i) the dissolution rate constant equals to: $k_d(\text{mol cm}^{-2} \text{ s}^{-1}) = 1.22 \times 10^{-8} \text{Exp}\left(-\frac{9418}{RT}\right)$;

(ii) the corrosion rate, for pure dissolution domain, in pipe geometry as a function of the flow velocity, V (m s^{-1}), the pipe diameter d_{pipe} (m), the temperature, T (K) and the dissolved iron concentration in the Pb-Bi bulk $C_{\text{Fe}}^{\text{LBE}}$ (b) (mol cm^{-3}):

$$\frac{dh}{dt}(\text{mm/year}) = \frac{V^{0.86} \text{Exp}\left(-\frac{3540.57}{T}\right) (3.544 \times 10^{-2} T - 303.3)}{-1.22 \times 10^{-4} d_{\text{pipe}}^{0.14} \frac{\text{Exp}\left(\frac{10484.97}{T}\right)}{(11065 - 1.293T)^{0.53}} + 1.01 \times 10^{-3} V^{0.86} (1.293T - 11065) \text{Exp}\left(-\frac{2407.78}{T}\right)}$$

(37)

With, V in (m/s), d_{pipe} in (m), T in (K).

This model can only be used for pure dissolution domain, not for a mixed phenomenon. However, the obtained reaction rate constant, k_d , can be used in other models, for pure dissolution domain but other geometry, for mixed process or for loop experiments. It is worth noting that this k_d value is obtained for average corrosion rate on sample that has some heterogeneous corrosion due to heterogeneous incubation times. To take into account localized corrosion, this value is slightly underestimated.

Acknowledgment:

Authors want to acknowledge EUROTRANS/DEMETRA European project for its financial support together with CEA TECNA project.

Authors thanks J.Pacio from KIT for his precious help in mass transfer modelling, M.Tabarant and H.Badgi from CEA Saclay/SEARS/ for ICP-AES measurements and S.Gosse from CEA Saclay/SCCME/LM2T for Thermocalc calculation.

References

- [1] C. Schroer, J. Konys, T. Furukawa, K. Aoto, *Journal of Nuclear Materials* 398 (2010) 109
 [2] C. Schroer, A Skrypnik, O. Wedemeyer, J. Konys, *Corrosion Science* 61 (2012) 63

- [3] F.J. Martín-Muñoz, L. Soler-Crespo, D. Gómez-Briceño, *Journal of Nuclear Materials* 416 (2011) 87
- [4] Y. Dai, W. Gao, T. Zhang, E. Platacis, S. Heinitz, K. Thomsen, *Journal of Nuclear Materials* 431 (2012) 113
- [5] A. Doubkova, F. Di Gabriele, P. Brabec, E. Keilova, *Journal of Nuclear Materials* 376 (2008) 260
- [6] O. I. Eliseeva, V. P. Tsisar, V. M. Fedirko, Ya. S. Matychak, *Materials Science*, 40 2 (2004) 260
- [7] O. I. Eliseeva, V. P. Tsisar, *Materials Science*, 43 2 (2007) 230
- [8] T Furukawa, G Müller, G Schumacher, A Weisenburger, A Heinzl, F Zimmermann, K Aoto, *Journal of Nuclear Science and Technology*, 41 3 (2004) 265
- [9] F. Gnecco, E. Ricci, C. Bottino, A. Passerone, *Journal of Nuclear Materials* 335 (2004) 185
- [10] I. V. Gorynin, G. P. Karzov, V. G. Markov, V. A. Yakovlev, *Metal Science and Heat Treatment*, 41 9 (1999) 384
- [11] P. Hosemann, R. Dickerson, P. Dickerson, N. Li, S.A. Maloy, *Corrosion Science* 66 (2013) 196
- [12] P. Hosemann, M.E. Hawley, D. Koury, J. Welch, A.L. Johnson, G. Mori, N. Li, S.A. Maloy, *Journal of Nuclear Materials* 381 (2008) 211
- [13] P. Hosemann, M. Hawley, G. Mori, N. Li, S.A. Maloy, *Journal of Nuclear Materials* 376 (2008) 289
- [14] M. Kondo, M. Takahashi, S. Yoshida, *Proceedings of ICAPP'04*, Pittsburgh USA, June 13-17 2004, paper 4044
- [15] Y. Kurata, M. Futakawa, S. Saito, *Journal of Nuclear Materials* 373 (2008) 164
- [16] Y. Kurata, M. Futakawa, S. Saito, *Journal of Nuclear Materials* 343 (2005) 333
- [17] Y. Kurata, *Journal of Nuclear Materials* 415 (2011) 254
- [18] K. Lambrinou, V. Koch, G. Coen, J. Van den Bosch, C. Schroer, *Journal of Nuclear Materials* 450 (2014) 244
- [19] J. Lim, H O. Nam, I S Hwang, *Proceedings of ICAPP'04*, Anaheim, CA USA, June 8-12, 2008, paper 8218
- [20] F.J. Martín-Muñoz, L. Soler-Crespo, D. Gómez-Briceño, *Journal of Nuclear Materials* 416 (2011) 87

- [21] G.Müller, A.Heinzel, J.Konys, G.Schumacher, A.Weisenburger, F.Zimmermann, V.Engelko, A.Rusanov, V.Markov, *Journal of Nuclear Materials* 335 (2004) 163
- [22] AK Rivai, M Takahashi, *Journal of Nuclear Materials* 398 (2010) 139
- [23] D. Sapundjiev, S. Van Dyck, W. Bogaerts, *Corrosion Science* 48 (2006) 577
- [24] C Schroer, A Skrypnik, O Wedemeyer, J Konys, *Corrosion Science* 61 (2012) 63
- [25] C Schroer, J Konys, *Journal of Engineering for Gas Turbines and Power*, 132 (2010) 082901
- [26] C. Schroer, J. Konys, T. Furukawa, K. Aoto, *Journal of Nuclear Materials* 398 (2010) 109
- [27] C Schroer, O Wedemeyer, A Skrypnik, J Novotny, J Konys, *Journal of Nuclear Materials* 431 (2012) 105
- [28] C Schroer, O Wedemeyer, J Novotny, A Skrypnik, J Konys, *Nuclear Engineering and Design* 280 (2014) 661
- [29] M.P. Short, R.G. Ballinger, H.E. Hänninen, *Journal of Nuclear Materials* 434 (2013) 259
- [30] L. Tan, M.T. Machut, K. Sridharan, T.R. Allen, *Journal of Nuclear Materials* 371 (2007) 161
- [31] A. Weisenburger, A. Heinzel, G. Müller, H. Muscher, A. Rousanov, *Journal of Nuclear Materials* 376 (2008) 274
- [32] A. Weisenburger, C. Schroer, A. Jianu, A. Heinzel, J. Konys, H. Steiner, G. Muller, C. Fazio, A. Gessi, S. Babayan, A. Kobzova, L. Martinelli, K. Ginestar, F. Balbaud-Celerier, F.J. Martin-Munoz, L. Soler Crespo, *Journal of Nuclear Materials* 415 (2011) 260
- [33] O. Yeliseyeva, V. Tsisar, G. Benamati, *Corrosion Science* 50 (2008) 1672
- [34] J Zhang, N Li, Y Chen, A.E. Rusanov, *Journal of Nuclear Materials* 336 (2005) 1
- [35] J.-L. Courouau, J.-C. Robin, *Journal of Nuclear Materials* 335 (2004) 264
- [36] L.Martinelli, J.L.Courouau, F.Balbaud-Célérier, *Nuclear Engineering and Design* 241 (2011) 1288
- [37] L. Martinelli, F. Balbaud-Célérier, A. Terlain, S. Delpech, G. Santarini, J. Favergeon, G. Moulin, M. Tabarant, G. Picard, *Corrosion Science* 50 (2008) 2523
- [38] L. Martinelli, T. Dufrenoy, K. Jaakou, A. Rusanov, F. Balbaud-Célérier, *Journal of Nuclear Materials* 376 (2008) 282
- [39] OECD/NEA Nuclear Science Committee, ISBN 978-92-64-99002-9, 2007 OCDE/AEN (2015), Handbook on Lead-bismuth Eutectic Alloy and Lead Properties, Materials

- Compatibility, Thermalhydraulics and Technologies, Nuclear Science, Éditions OCDE, Paris, <https://doi.org/10.1787/42dcd531-en>.
- [40] F. Balbaud-Célérier, A. Terlain, *Journal of Nuclear Materials* 335 (2004) 204
- [41] F. Balbaud-Célérier, L. Martinelli, *Journal of Engineering for Gas Turbines and Power* 132, (2010) 102912
- [42] L. Martinelli, F. Balbaud-Célérier, V. Botton, C. Alémany-Dumont, *submitted to International Communication on Heat and Mass Transfer*
- [43] E. Yamaki, K. Ginestar, L. Martinelli, *Corrosion Science* 53 (2011) 3075
- [44] M. Roy, L. Martinelli, K. Ginestar, J. Favergeon, G. Moulin, *Journal of Nuclear Materials* 468 (2016) 153
- [45] L. Martinelli, F. Balbaud-Célérier, *Materials and Corrosion*, 62 6 (2011) 531
- [46] L. Martinelli, F. Balbaud-Célérier, G. Picard, G. Santarini, *Corrosion Science* 50 (2008) 2549
- [47] H. Chen, Y. Chen, J. Zhang, *Progress in Nuclear Energy* 50 (2008) 587
- [48] A. Arkundato, Z. Su'ud, M. Abdullah, W. Sutrisno, Massimo Celino, *Annals of Nuclear Energy* 62 (2013) 298
- [49] B. X. He, N. Li, M. Mineev, *Journal of Nuclear Materials*, 297 (2001) 214
- [50] K.-C. Lan, Y. Chen, T.-C. Hung, H.-M. Tung, G.-P. Yu, *Computational Materials Science* 77 (2013) 139
- [51] M. L. Machut, K. Sridharan, N. Li, S. Ukai, T. Allen, *Journal of Nuclear Materials* 371 (2007) 134
- [52] T. Malkow, H. Steiner, H. Muscher, J. Konys, *Journal of Nuclear Materials* 335 (2004) 199
- [53] A. Maulana, Z. Su'ud, K. D. Hermawan, Khairurrijal, *Progress in Nuclear Energy* 50 (2008) 616
- [54] K. Mikityuk, *Nuclear Engineering and Design* 240 (2010) 3632
- [55] J. Zhang, N. Li, *Journal of Nuclear Materials* 321 (2003) 184
- [56] J. Zhang, N. Li, *Journal of Nuclear Materials* 326 (2004) 201
- [57] F. P. Berger, K.-F.-L. Hau, *International Journal of Heat and Mass Transfer* 20 (1977) 1185
- [58] P. Harriott, R. M. Hamilton, *Chemical Engineering Science*, 20 (1965) 1073
- [59] D. C. Silverman, *Corrosion*, 60 11 (2004) 1003
- [60] M. Eisenberg, C. W. Tobias, C. R. Wilke, *Journal of the Electrochemical Society*, 101 (1954) 306
- [61] L. Labraga, N. Bourabaa, T. Berkah, *Experiments in fluids*, 33 (2002) 488

- [62] Globe, Dropkin, *Journal of Heat Transfer*, 81 1 (1959) 24
- [63] B.E.Lauder, G.J.Reece, W.Rodi, *Journal of Fluid Mechanics*, 68 3 (1975) 537
- [64] J.L. Courouau, *Journal of Nuclear Materials* 335 (2004) 254
- [65] V.Ghetta, F.Gamaoun, J.Fouletier, M.Hénault, A.Lemoulec, *Journal of Nuclear Materials*, 296 (2001) 295
- [66] W.M.Robertson, *Transactions of the Metallurgical Society of AIME*, 242 (1968) 2139
- [67] A.Bejan, *Convection Heat Transfer*, 3rd edition, ed. Wiley, 2004
- [68] F.Balraud-Célérier, L.Martinelli, *Journal of Engineering for Gas Turbines and Power*, 132 (2010) 102912-1
- [69] Martynov, P.N., Ivanov K.D., (1998), Nuclear heat application: design aspect and opening experiments. Proceedings of four technical meetings held between dec 1995 and apr 1998, 177-184
- [70] D.C.Silverman, *Corrosion*, 60, 11 (2004) 1003
- [71] D.C.Silverman, *Corrosion*, 40 (1984) 220
- [72] D.C.Silverman, *Corrosion*, 44 (1988) 42
- [73] D.C.Silverman, *Corrosion*, 55 (1999) 1115
- [74] R.Taillier, Internship report, Master MEGA, INSA Lyon, 2006

Table list

Table 1: T91 composition in weight percent (wt%). Iron is the balance.

Table 2: experimental conditions and results.

Table 3: dimension of the electrochemical cell used to experimentally determine the mass transfer coefficient in same geometry and Reynolds number as CICLAD.

Table 4: Parameters needed for modelling the corrosion rate in COLIMESTA and CICLAD devices.

Figures

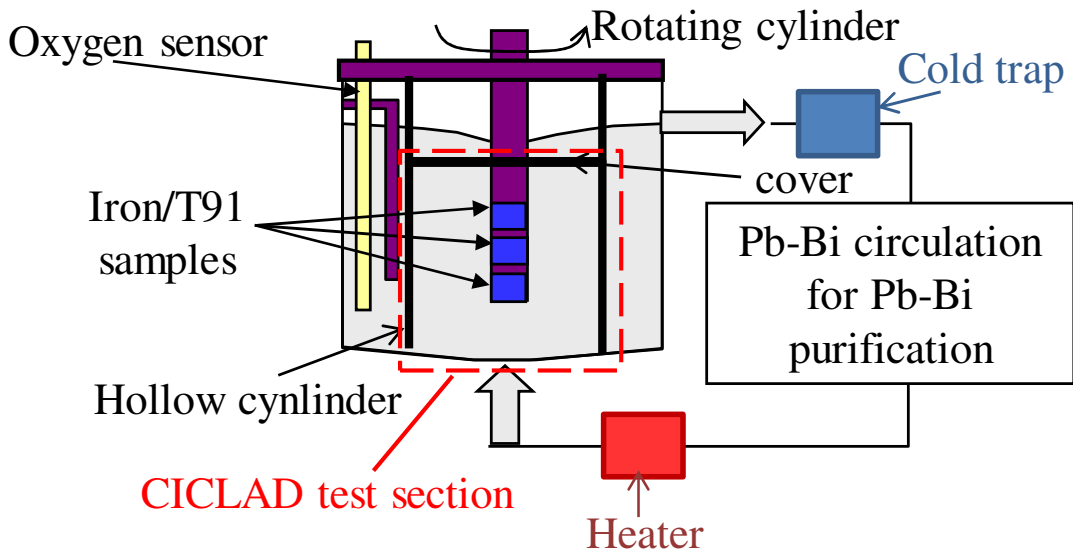


Figure 1. CICLAD diagram.

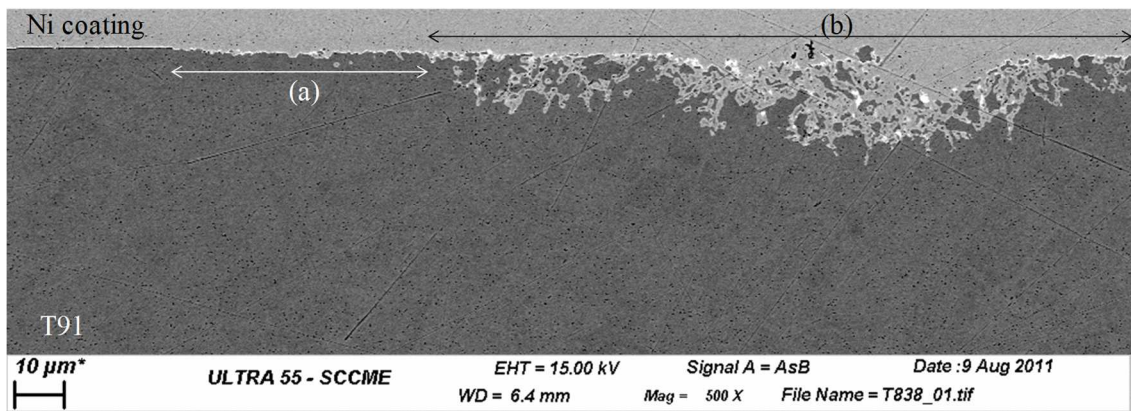


Figure 2. SEM picture of cross section of T91 corroded 400 h in COLIMESTA device at 552°C. Two zones, (a) and (b) are noticeable: (a) slight corrosion zone; (b) accelerated corrosion zone.

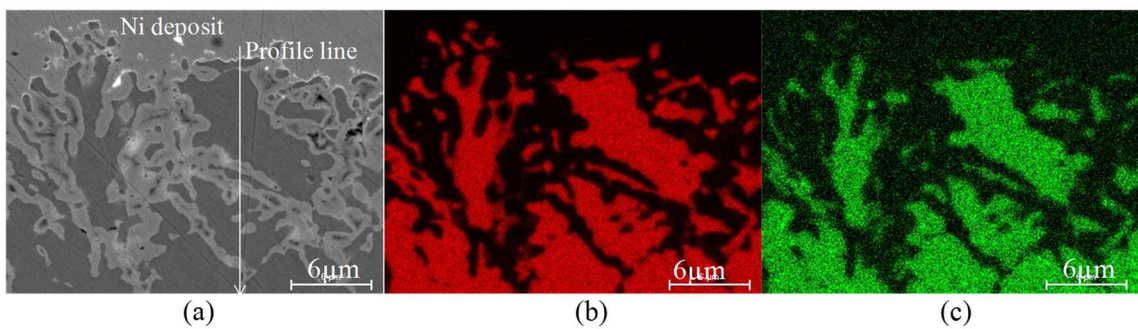


Figure 3. EDX map of an accelerated corrosion zone (see Figure 2b) of T91 corroded 400 h in COLIMESTA device at 552°C. (a) SEM-QBSD picture. The profile line corresponds to the EDX profile of Figure 4; (b) Fe map; (c) Cr map.

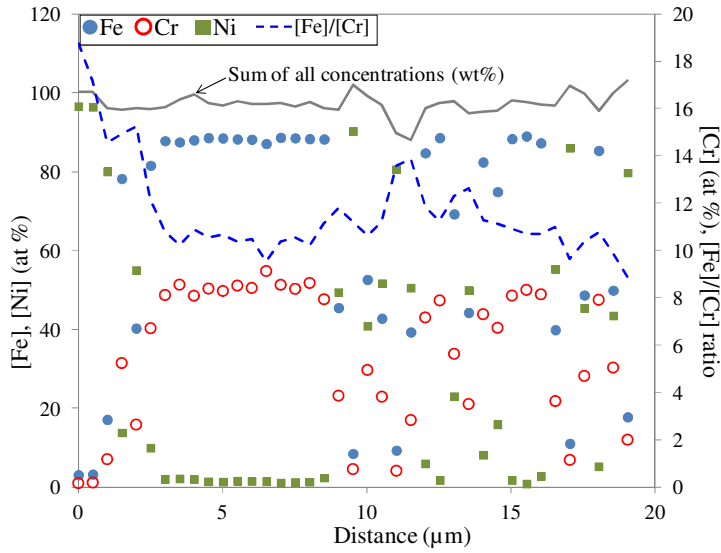


Figure 4. EDX profile of profile line presented on Figure 3a. Presence of Ni corresponds to Ni deposit performed after test.

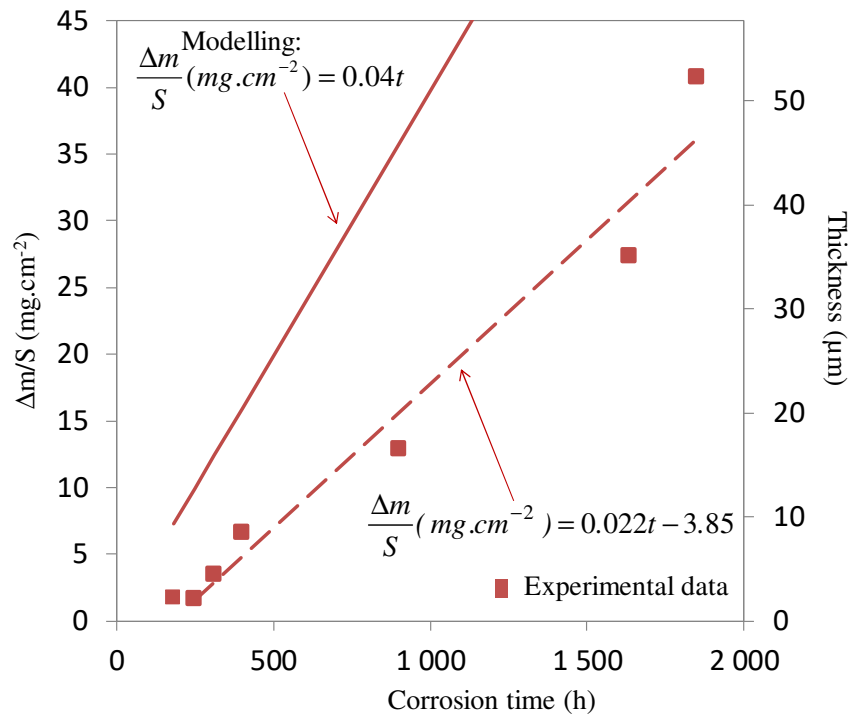


Figure 5. T91 weight loss per surface area (mg cm^{-2}) or T91 dissolved thickness (μm) towards time (h). Experiment performed in COLIMESTA at 552°C . Modelling is performed considering pure mass transfer control.

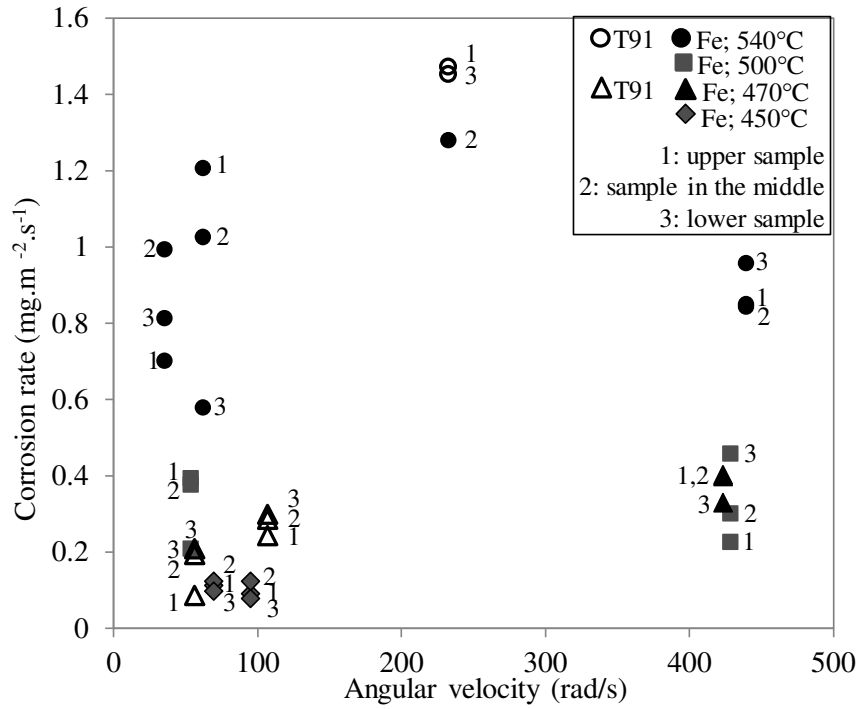
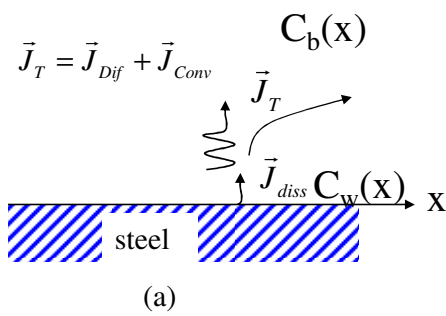


Figure 6. Corrosion rate ($\text{mg m}^{-2} \text{s}^{-1}$) of T91 and pure iron at 450, 470, 500 and 540°C . Open symbols correspond to T91 samples, full symbols to pure Fe samples. Numbers 1, 2, 3 correspond respectively to the upper sample, the sample in the middle and the lower sample on the rotating shaft.

$C_w(x)$: iron concentration at the wall surface
 $C_b(x)$: iron concentration in the bulk



δ : thickness of the boundary layer

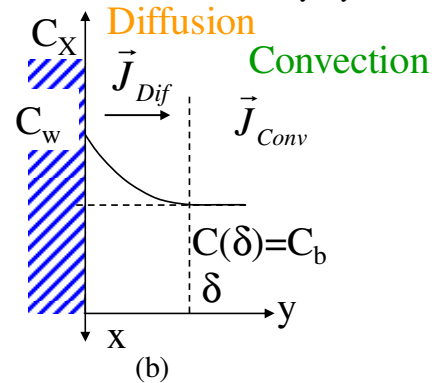


Figure 7. (a) diagram of the 3 fluxes involved in dissolution process [66] (b) diagram representing iron concentration gradient in the diffusion boundary layer.

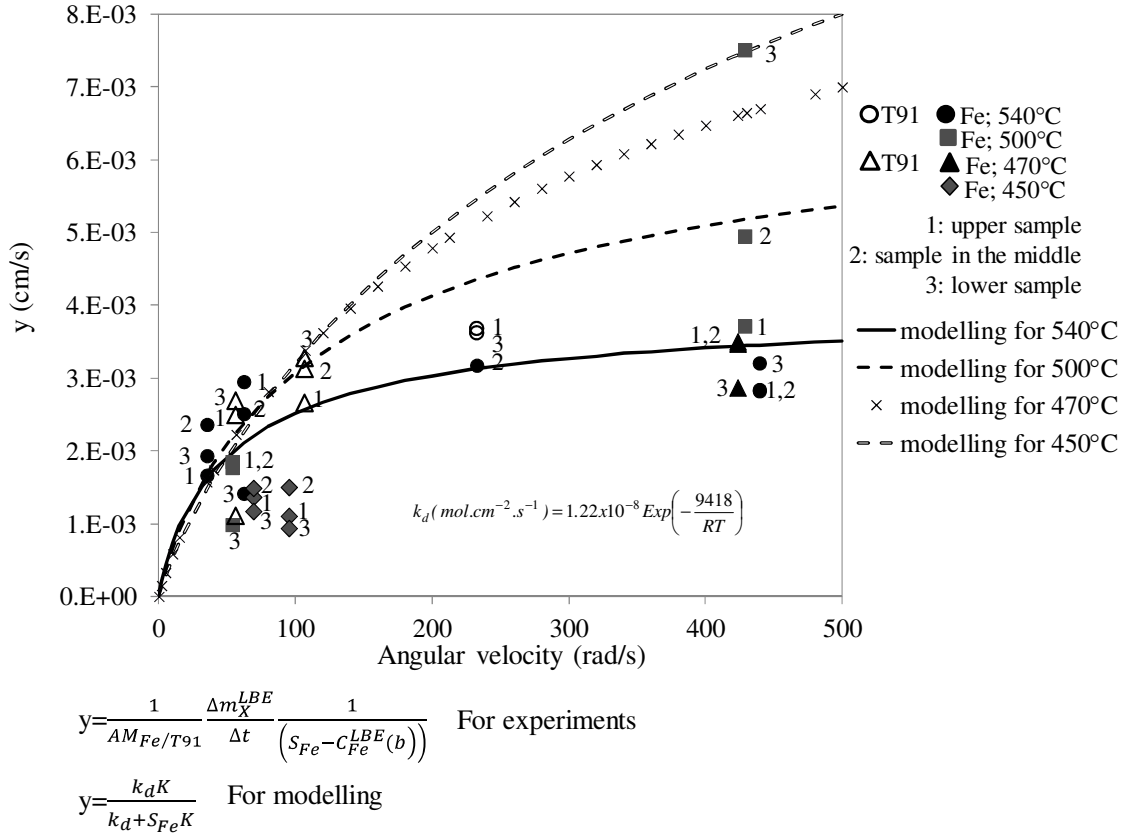


Figure 8. Corrosion rate at various temperatures (from Figure 6) divided by the difference between iron solubility limit and iron concentration in the LBE bulk $\left(\frac{1}{AM_{Fe/T91}} \frac{\Delta m_X^{LBE}}{\Delta t} \frac{1}{(S_{Fe} - C_{Fe}^{LBE}(b))}\right)$ as a function of angular velocity. Modelling $\left(\frac{k_d K}{k_d + S_{Fe} K}\right)$ for the various temperatures (450, 470, 500, 540°C).

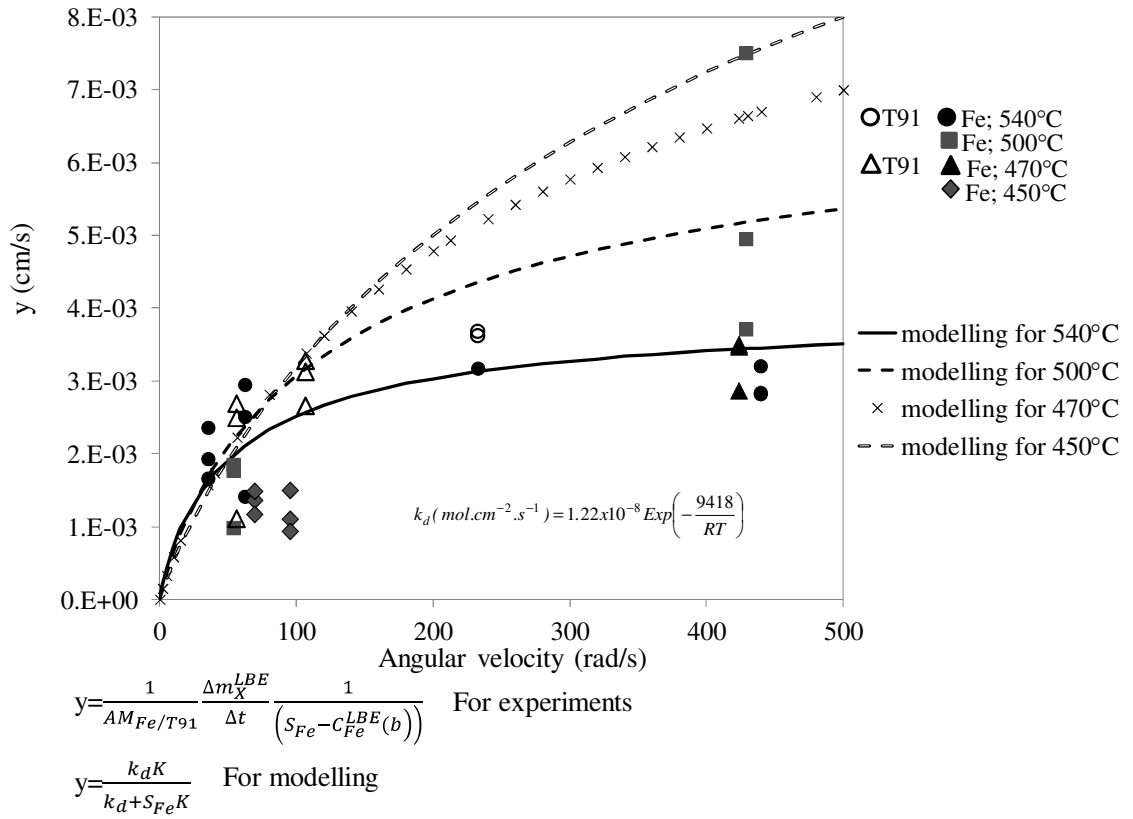


Figure 9. Corrosion rate at various temperatures (from Figure 6) divided by the difference between iron solubility limit and iron concentration in the LBE bulk $\left(\frac{1}{AM_{Fe/T91}} \frac{\Delta m_X^{LBE}}{\Delta t} \frac{1}{(S_{Fe} - C_{Fe}^{LBE}(b))}\right)$ as a function of angular velocity. Modelling $\left(\frac{k_d K}{k_d + S_{Fe} K}\right)$ for the various temperatures (450, 470, 500, 540°C). K is given only by equation (27) on the overall range of $Re^2 Sc$, i.e. of angular velocity ω k_d is given by the previous fit:

$$k_d (mol\ cm^{-2}\ s^{-1}) = 1.22 \times 10^{-8} \text{Exp}\left(-\frac{9418}{RT}\right).$$

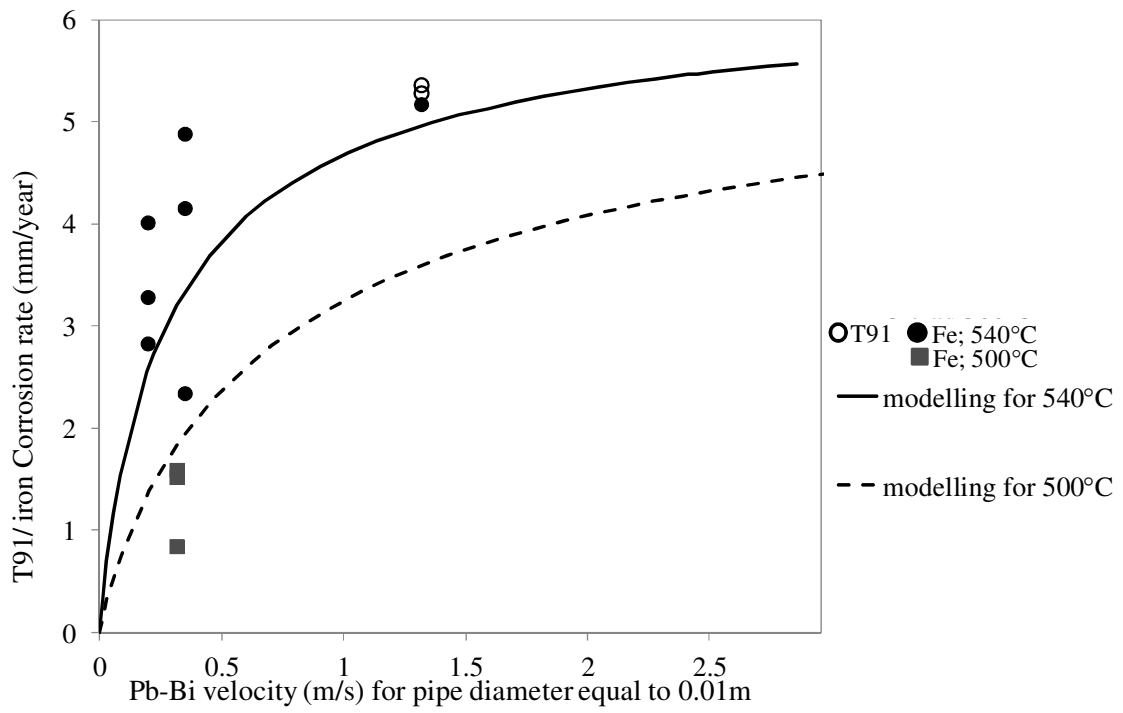


Figure 10. Corrosion rate at 500°C and 540°C (from Figure 9) as a function of pipe velocity.

Modelling, $\frac{dh}{dt}$ (mm/year), considering relation (37).

	Cr	Mo	Si	Ni	Cu	Nb	V	Mn	C	P	S	Sn	Al
T91	9.25	0.89	0.22	0.11	0.06	0.06	0.21	0.38	0.1025	0.021	-	-	-
Fe	0.03	<0.005	<0.01	0.03	0.04	-	-	0.43	0.012	0.015	0.024	<0.01	0.05

Table 1: Table 1: T91 and Fe compositions in weight percent (wt%). Iron is the balance.

Experiment number /Material	Temperature (°C)	Experimental corrosion rate (mg m ⁻² s ⁻¹)	Angular velocity (rad/s)	Corrosion duration (h)	Dissolved oxygen concentration (wt%)	Dissolved Fe concentration in LBE bulk (mol m ⁻³)
1 / Fe	400	3.41.10 ⁻³	424	335	2.10 ⁻⁹	4.57.10 ⁻²
2 / Fe	399	3.13.10 ⁻³	423	393	4.10 ⁻¹⁵	5.40.10 ⁻⁴
3 / Fe	450	1.12.10 ⁻¹	69	235	4.10 ⁻¹⁰	1.82.10 ⁻²
3 / Fe	450	1.22.10 ⁻¹	69	235	4.10 ⁻¹⁰	1.82.10 ⁻²
3 / Fe	450	9.58.10 ⁻²	69	235	4.10 ⁻¹⁰	1.82.10 ⁻²
4 / Fe	450	9.01.10 ⁻²	95	142	2.10 ⁻¹⁰	1.82.10 ⁻²
4 / Fe	450	1.22.10 ⁻¹	95	142	2.10 ⁻¹⁰	1.82.10 ⁻²
4 / Fe	450	7.66.10 ⁻²	95	142	2.10 ⁻¹⁰	1.82.10 ⁻²
5 / T91	470	2.17.10 ⁻¹	107	500	9.10 ⁻¹⁴	6.53.10 ⁻²
5 / T91	470	2.56.10 ⁻¹	107	500	9.10 ⁻¹⁴	6.53.10 ⁻²
5 / T91	470	2.67.10 ⁻¹	107	500	9.10 ⁻¹⁴	6.53.10 ⁻²
6 / T91	467	7.65.10 ⁻²	56	790	3.10 ⁻¹⁴	7.65.10 ⁻²
6 / T91	467	1.72.10 ⁻¹	56	790	3.10 ⁻¹⁴	7.65.10 ⁻²
6 / T91	467	1.86.10 ⁻¹	56	790	3.10 ⁻¹⁴	7.65.10 ⁻²
7 / T91	469	1.66.10 ⁻²	212	305	10 ⁻¹³	2.71.10 ⁻²
8 / Fe	471	4.01.10 ⁻¹	423	386	3.10 ⁻¹⁵	3.63.10 ⁻²
8 / Fe	471	3.98.10 ⁻¹	423	386	3.10 ⁻¹⁵	3.63.10 ⁻²
8 / Fe	471	3.29.10 ⁻¹	423	386	3.10 ⁻¹⁵	3.63.10 ⁻²
9 / Fe	500	2.26.10 ⁻¹	429	456	3.10 ⁻¹⁴	2.89.10 ⁻¹
9 / Fe	500	3.01.10 ⁻¹	429	456	3.10 ⁻¹⁴	2.89.10 ⁻¹
9 / Fe	500	4.57.10 ⁻¹	429	456	3.10 ⁻¹⁴	2.89.10 ⁻¹
10 / Fe	498	3.94.10 ⁻¹	54	68	2.10 ⁻⁹	4.52.10 ⁻³
10 / Fe	498	3.76.10 ⁻¹	54	68	2.10 ⁻⁹	4.52.10 ⁻³
10 / Fe	498	2.09.10 ⁻¹	54	68	2.10 ⁻⁹	4.52.10 ⁻³
11 / T91	540	1.32	232	168	9.10 ⁻¹³	4.04.10 ⁻²
11 / Fe	540	1.28	232	168	9.10 ⁻¹³	4.04.10 ⁻²
11 / T91	540	1.31	232	168	9.10 ⁻¹³	4.04.10 ⁻²
12 / Fe	550	8.48.10 ⁻¹	439	264	3.10 ⁻¹³	3.43.10 ⁻¹
12 / Fe	550	8.43.10 ⁻¹	439	264	3.10 ⁻¹³	3.43.10 ⁻¹
12 / Fe	550	9.57.10 ⁻¹	439	264	3.10 ⁻¹³	3.43.10 ⁻¹
13 / Fe	539	1.21	62	24	10 ⁻⁸	1.79.10 ⁻²
13 / Fe	539	1.03	62	24	10 ⁻⁸	1.79.10 ⁻²
13 / Fe	539	5.80.10 ⁻¹	62	24	10 ⁻⁸	1.79.10 ⁻²
14 / Fe	540	7.00.10 ⁻¹	35	28	10 ⁻⁸	0
14 / Fe	540	9.93.10 ⁻¹	35	28	10 ⁻⁸	0
14 / Fe	540	8.13.10 ⁻¹	35	28	10 ⁻⁸	0

Table 2: Experimental conditions and results in CICLAD facility.

Sample material	Fe	T91
M_M (g/mol)	56	55.08
S_{Fe} (mol/m ³)	$18.27 \exp\left(-\frac{10085.3}{T}\right)(11065 - 1.293T)$	
D_{Fe}^{Pb} (m ² /s)	$4.898 \times 10^{-7} \exp\left(-\frac{43934.77}{RT}\right)$	
ν_{LBE} (m ² /s)	$\frac{4.94 \times 10^{-4}}{11065 - 1.293T} \exp\left(\frac{754.1}{T}\right)$	

Table 3: Parameters needed for modelling the corrosion rate in COLIMESTA and CICLAD devices.